



Enhanced thermoelectric power near the quantum phase transition in the itinerant-electron ferromagnet MnSi

J.-G. Cheng, F. Zhou, J.-S. Zhou,* and J. B. Goodenough
Texas Materials Institute, University of Texas at Austin, Austin, Texas 78712, USA

Y. Sui

Center for Condensed Matter Science and Technology, Department of Physics, Harbin Institute of Technology, Harbin 150001, China

(Received 18 September 2010; published 1 December 2010)

The itinerant-electron ferromagnet MnSi is a well-known example that shows a transition from Fermi-liquid $\Delta\rho \propto T^2$ to non-Fermi-liquid (NFL) $\Delta\rho \propto T^{3/2}$ behavior when the spiral ferromagnetic transition $T_c \approx 29$ K at ambient pressure is suppressed to zero by the application of hydrostatic pressures above $P_c \approx 14.6$ kbar. Several experimental probes have been employed to reveal the intriguing properties near P_c . In this paper, we report the temperature dependence of thermoelectric power $S(T)$ under hydrostatic pressures up to 20 kbar on a single crystal of MnSi. At pressures close to P_c , we observed at low temperatures an unusual enhancement of $S(T)$, which can be described well with the relationship $S/T \propto \ln(1/T)$, a formula that has been proposed to describe a system as a quantum critical point (QCP) is approached. The relationship has previously been observed in systems close to a magnetic QCP, for example, $\text{La}_{1.6-x}\text{Nd}_{0.4}\text{Sr}_x\text{CuO}_4$ ($x=0.24$). The enhancement of thermoelectric power in MnSi occurs at a temperature above the NFL phase and over a broad pressure range around P_c .

DOI: [10.1103/PhysRevB.82.214402](https://doi.org/10.1103/PhysRevB.82.214402)

PACS number(s): 71.27.+a, 72.20.Pa, 75.40.Cx, 75.47.-m

The itinerant-electron ferromagnet MnSi with the cubic B20 structure has been extensively studied under high pressure since T_c can be completely suppressed above $P_c \approx 1.5$ GPa; this pressure level can be easily achieved in a liquid- or gas-filled, large-volume pressure device.¹⁻¹⁰ These devices not only make neutron scattering under pressure possible but they also allow reliable measurements of transport and magnetic properties under hydrostatic pressure. Measurements have revealed in great detail the low-temperature phase transition as T_c approaches zero. At ambient pressure, MnSi exhibits a ferromagnetic order with a small spiral spin antiferromagnetic component below $T_c \approx 29$ K characterized by a left-handed helical twist with a periodicity of 180 Å propagating along the [111] direction.¹¹ Such a helical modulation of spin structure is due to a combination of a strong ferromagnetic exchange interaction and a relatively weak Dzyaloshinskii-Moriya spin-orbit interaction resulting from the noncentrosymmetric crystal structure P2₁3.^{12,13} In the ferromagnetically ordered metallic phase, the resistivity $\rho(T)$ at low temperature follows a power law $\Delta\rho = \rho - \rho_0 \propto T^2$, characteristic of a Fermi-liquid (FL) phase. T_c has been well mapped as a function of pressure based on data from several groups. These high-pressure studies were motivated to explore the effect of quantum fluctuations on physical properties at low temperatures as ferromagnetic spin ordering is suppressed. Figure 1 shows a schematic drawing of the existing T - P phase diagram of MnSi. The second-order ferromagnetic transition at T_c decreases roughly linearly as pressure increases to $P^* \approx 12$ kbar; above P^* , T_c drops much more dramatically with P and the transition becomes weakly first order for $P > P^*$, T_c approaching zero at $P_c \approx 14.6$ kbar. However, instead of a quantum critical point (QCP), which is defined where a second-order magnetic transition vanishes, high pressure here induces a transition from a spin-ordered phase to a partially spin-ordered or spin-

textured phase at $P \geq P_c$. The spin-textured phase has been characterized by a broad scattering intensity around the [110] direction in reciprocal space by neutron inelastic scattering below T_0 ,³ which is roughly on the line extrapolated from T_c versus P for $P < P^*$. This partially spin-ordered phase is associated with strong two-dimensional (2D) spin fluctuations. However, the low-temperature phase at $P > P_c$ is more complicated than that detected by the neutron inelastic scattering. For the phase at $P > P_c$, the ac magnetic susceptibility $\chi_{ac}(T)$ shows a broad maximum at $T_m > T_0$; T_m is nearly independent of pressure and the $\chi_{ac}(T)$ with a broad maximum can still be tracked up to $P=30$ kbar.² The most dramatic change on crossing P_c is an abrupt transition from a Fermi liquid to a non-FL (NFL) $T^{3/2}$ dependence in the temperature dependence of the resistivity.¹⁴

The NFL phase in the T - P phase diagram in the literature as reproduced in Fig. 1 has been defined within pressure and temperature ranges $P > P_c$ and $T < T_m$. However, $\Delta\rho(T)$

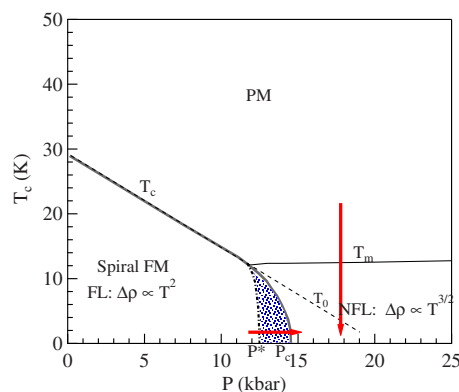


FIG. 1. (Color online) A schematic phase diagram of MnSi. See text for the definitions of critical temperatures and pressures.

starts to deviate from the $T^{3/2}$ dependence as temperature increases at a much lower temperature than T_m . Since T_c is terminated with a phase transition to a partially magnetically ordered phase at $P=P_c$, quantum critical fluctuations associated with a QCP have not been expected. Instead, the $T^{3/2}$ dependence of the resistivity in the NFL phase has been interpreted by a model considering the spin texture.¹⁵ Although the spin-textured phase as detected by neutron inelastic scattering is confined to below T_0 , whether the profile of T_0 versus P matches the area where the $T^{3/2}$ dependence is found, has not been confirmed. As the NFL phase is approached at low temperatures from the FL phase by tuning pressure (the path is shown in Fig. 1 by a horizontal arrow), the change at P_c is clearly a quantum phase transition. Alternatively, the NFL phase can also be approached from the paramagnetic phase under $P>P_c$ by lowering temperature; the path is shown as a vertical arrow in Fig. 1. In this case, thermally driven critical fluctuations as well as quantum spin fluctuations are expected to be reflected in physical properties. Whereas the $T^{3/2}$ dependence of the resistivity may be explained by the model of a spin-textured phase below T_0 , the cause for a hump in $\chi_{ac}(T)$ at T_m remains unknown. As seen in several other cases where a QCP is approached under pressure or by applying a magnetic field, thermoelectric power is enhanced by quantum critical fluctuations at low temperatures. These observations motivated us to carry out thermoelectric-power measurements on a single-crystal sample of MnSi under high pressure to 20 kbar. We have demonstrated a remarkable enhancement in the thermoelectric power in the paramagnetic phase under a broad range of pressure around P_c .

The MnSi single crystal in this study was grown by melting a polycrystalline sample. At first, the polycrystalline MnSi samples were prepared by sintering a stoichiometric mixture of high-purity Mn and Si powders at 700 °C for 30 h in a vacuum-sealed quartz tube ($<10^{-5}$ torr). Then, the single-crystal sample was obtained by heating the obtained polycrystalline sample to 1280 °C for 4 days before slowly cooling down to room temperature. The single-crystal sample was characterized by both powder X-ray diffraction (XRD) and single-crystal Laue backdiffraction techniques. The lattice parameter $a=4.5607(9)$ Å refined from the powder XRD is in excellent agreement with that reported in the literature.^{16,17} A clear Laue backdiffraction pattern with large and round spots confirms the good quality of the single crystal. The sample quality was further checked by a resistivity measurement in the temperature range from 5 to 300 K with a four-probe method at ambient pressure. As shown in Fig. 2(b); the residual resistivity $\rho(T \rightarrow 0)$ and the residual resistivity ratio [$RRR=\rho(300\text{ K})/\rho(0\text{ K})$] are $1.74\ \mu\Omega\text{ cm}$ and 100, respectively. dc magnetic susceptibility was measured with a superconducting quantum interference device magnetometer (Quantum Design). Specific-heat measurements were carried out with a 2τ relaxation method in a physical properties measurement system (Quantum Design). Thermal conductivity was measured with a steady-state method. Thermoelectric power measurements under hydrostatic pressures were performed in a homemade, self-clamped piston-cylinder device. Daphne oil 7373 was used as a pressure

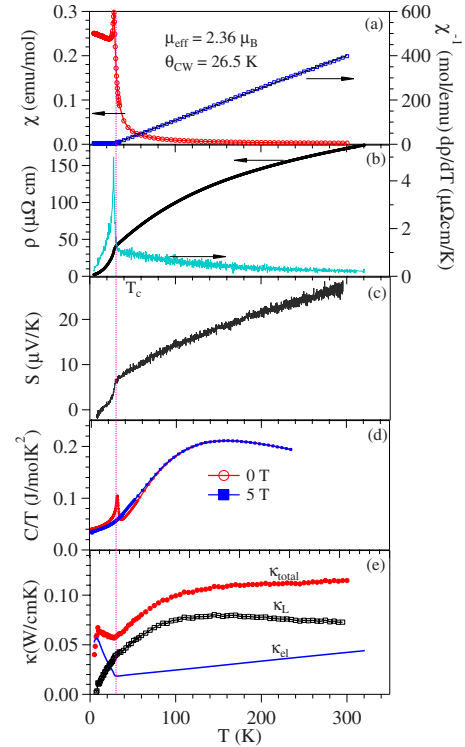


FIG. 2. (Color online) Temperature dependence of physical properties of MnSi measured at ambient pressure: (a) magnetic susceptibility $\chi(T)$ and its inverse measured under a magnetic field $H=100$ Oe in zero-field cool. A Curie-Weiss fitting has been applied in the paramagnetic phase as shown by the solid line. (b) Resistivity $\rho(T)$ and its derivative $d\rho/dT$. (c) thermoelectric power $S(T)$. (d) Specific heat divided by temperature C/T under $H=0$ and 5 T. (e) Thermal conductivity $\kappa(T)$. The lattice contribution κ_L was calculated by subtracting the electronic part $\kappa_{el}=LT/\rho$ from the total thermal conductivity κ_{total} .

medium. A manganin coil has been placed inside the pressure chamber, which serves as not only a pressure manometer but also a heater to build a temperature gradient across the sample for measuring thermoelectric power.¹⁸ The thermoelectric power measured with the high-pressure setup is about 20% smaller than that obtained with a device used at ambient pressure. However, they show the same temperature dependence. We have multiplied a constant factor to the $S(T)$ from the high-pressure setup based on the room-temperature value of S obtained with the setup at ambient pressure.

Figure 2 summarizes the physical properties of MnSi measured under ambient pressure below 300 K. While no thermal-conductivity data are available for comparison, all other data are consistent with those reported in the literature. It can be seen that all physical properties exhibit distinct features at $T_c \approx 28.5$ K as indicated by the vertical dotted line. Figure 2(a) shows the temperature dependence of the dc magnetic susceptibility $\chi(T)$ and its inverse measured under zero-field cooling with a magnetic field $H=100$ Oe. As observed in the ac magnetic susceptibility, a peak appears at T_c . Apparently, this peak is field-dependent and disappears completely at $H=5000$ Oe. A linear Curie-Weiss (CW) behavior is followed at the high-temperature paramagnetic region of $\chi^{-1}(T)$; CW fitting (solid line) yields an effective magnetic

moment $\mu_{\text{eff}}=2.36 \mu_B$ and Curie temperature $\theta_{\text{CW}}=26.5$ K. Based on a saturation moment $\mu_s=0.39 \mu_B$ extrapolated to $H=0$ T at 5 K (data are not shown here), we obtained a $\mu_{\text{eff}}/\mu_s \approx 6$, which is in agreement with a typical itinerant-electron ferromagnet. The metallic conductivity of MnSi is shown in Fig. 2(b), where a distinct drop in resistivity $\rho(T)$ and a sharp anomaly in $d\rho/dT$ can be clearly observed at T_c . Fitting to a power law $\rho(T)=\rho_0+AT^n$ below 20 K gives $\rho_0=1.74(2) \mu\Omega \text{ cm}$, $A=0.0178(5) \mu\Omega \text{ cm K}^{-2}$, and $n=2.2(1)$. These values are in excellent agreement with those reported by Mena *et al.*¹⁹ and confirm the FL behavior at ambient pressure. It is interesting to note that the $\rho(T)$ data exhibit a strong sublinear temperature dependence in a wide temperature interval above T_c , which has also been observed in the antiferromagnetic metal PdCrO₂,²⁰ indicative of the dominant role of spin fluctuations in scattering conduction electrons. The temperature dependence of the thermoelectric power $S(T)$ in Fig. 2(c) resembles very much that of $\rho(T)$ in the whole temperature range. But $S(T)$ exhibits a remarkably sharp drop at T_c . An abrupt change in $S(T)$ at T_c has been seen in metallic ferromagnets such as ZrZn₂ (Ref. 21) and SrRuO₃ (Ref. 22) in which thermally driven critical fluctuations are confined to a very small range in the reduced temperature $(T-T_c)/T_c$.²³ The $S(T)$ of MnSi does not show the phonon-drag effect typical of most metals. One possibility for a missing phonon-drag effect in $S(T)$ is that MnSi has a poor phonon transport. As seen in the thermal conductivity and its analysis, the short phonon mean free path may indeed be a major cause. Specific-heat $C_p(T)$ data measured under $H=0$ and 5 T are displayed in Fig. 2(d) as C_p/T versus T . The sharp λ -shaped anomaly at $H=0$ T spreads out over a broad temperature range around T_c under a magnetic field $H=5$ T; the same behavior has been observed in other ferromagnets, such as EuO (Ref. 24) and YTiO₃.²⁵ Close to values reported in a previous study,²⁶ the linear electronic specific-heat coefficient γ has been estimated to be about 41 mJ/mol K² and 37 mJ/mol K² at $H=0$ T and 5 T, respectively. In comparison with the calculated value $\gamma_0 \sim 1$ mJ/mol K² for an electron gas, the observed γ and thus the effective mass m^* of conduction electrons in MnSi have been largely enhanced. This enhancement is further confirmed through the Kadowaki-Woods ratio, A/γ^2 , A is from the power law $\rho(T)=\rho_0+AT^2$.²⁷ Based on the values of A and γ obtained at ambient pressure and 0 T, A/γ^2 was calculated to be $1.06 \times 10^{-5} \mu\Omega \text{ cm}(\text{mol K/mJ})^2$, which is in line with the universal value of $1.0 \times 10^{-5} \mu\Omega \text{ cm}(\text{mol K/mJ})^2$ for all other heavy-fermion compounds.²⁷ Measurements of thermal expansion²⁸ and lattice parameters^{4,29} all revealed a clear anomaly at T_c due to magnetostriction.

The thermal conductivity κ in Fig. 2(e) includes contributions from the lattice and the electrons as heat carriers in the highly conductive MnSi metal. A minimum of $\kappa(T)$ at T_c is reminiscent of spin critical scattering seen in other magnetic insulators.³⁰ However, after subtracting the electronic contribution $\kappa_{\text{el}}=LT/\rho$ according to the Wiedemann-Franz law with $L=2.44 \times 10^{-8} \text{ W } \Omega \text{ K}^{-2}$, the lattice contribution κ_L does not show any distinct anomaly near T_c . An attempt to fit κ_L with the Debye formula of phonon thermal conductivity failed; a low, nearly temperature-independent $\kappa_L(T)$ near room temperature suggests a glassy heat transport through

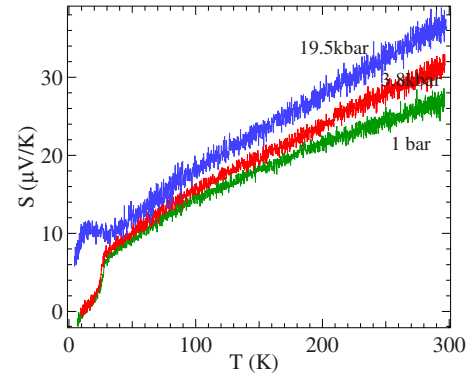


FIG. 3. (Color online) Typical temperature dependences of the thermoelectric power S of MnSi under three different pressures.

the MnSi lattice. This observation is consistent with the lack of a phonon-drag effect in the thermoelectric power at ambient pressure.

The pressure effect on $S(T)$ under three typical pressures is shown in Fig. 3. The curve under $P=3.8$ kbar was obtained after a loading force to 20 kbar was released. This curve is close to that at ambient pressure, which indicates that the sample and locations of electric leads and thermal couples have not been altered under pressure to 20 kbar. This figure also shows that the most dramatic pressure effect on $S(T)$ occurs at low temperatures. The low-temperature $S(T)$ curves under all pressures obtained in this work are shown in Fig. 4. As mentioned above, the T_c of MnSi can be monitored by the sudden drop of $S(T)$. There are several important features in the $S(T)$ data under pressure: (1) consistent with all other measurements under pressure, T_c was suppressed gradually from 28.5 K at 1 bar to ~ 10 K under 13.1 kbar, but it cannot be identified from the $S(T)$ under $P > 13.1$ kbar; (2) the $S(T)$ data and black lines, which are guides to eyes, show that S varies linearly as a function of temperature over a wide temperature range from 100 K down to a temperature close to T_c ; (3) an obvious upturn of $S(T)$ develops for $P \geq 9$ kbar at a $T_i \geq T_c$ as temperature decreases; (4) the low-temperature enhancement is terminated by a sharp drop of S at T_c in the pressure range $9 \leq P$

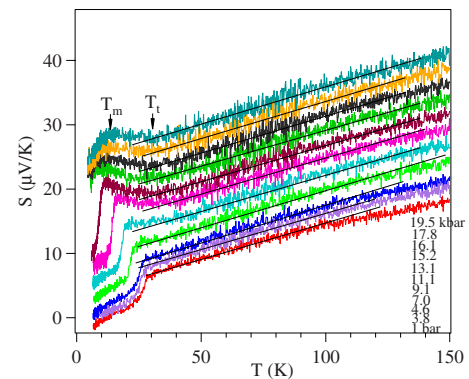


FIG. 4. (Color online) The low-temperature $S(T)$ for all pressures in this work. Lines inside the figure are guides for eyes. All curves except that for 1 bar have been shifted vertically for clarification.

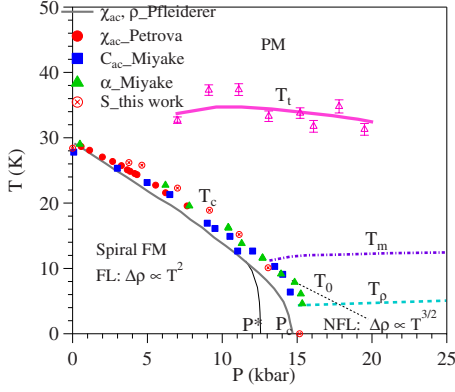


FIG. 5. (Color online) The phase diagram of MnSi which includes critical temperatures obtained in this work together with data from Refs. 2, 8, 9, 26, and 28.

< 15 kbar where T_c still exists; (5) $S(T)$ develops into a broad hump with the maximum located at a T_m above $P \geq 15$ kbar where T_c is suppressed to zero temperature. By mapping out T_c , T_m , and T_t as a function of pressure, we can plot an update of the T - P phase diagram together with data from the literature in Fig. 5. The variation with pressure of T_c in the present study agrees well with the established phase diagram based on various techniques including resistivity, ac magnetic susceptibility, ac specific heat, and thermal expansion. It should be noted that T_t emerges at a pressure much lower than P_c and $P^* \approx 12$ kbar where the transition has been reported to change from second order to weakly first order.³¹ The transition on crossing P^* has been sensitively picked up by the ac magnetic susceptibility, which is a transition from a gradual increase at T_c for $P < P^*$ to an abrupt increase in $\chi_{ac}(T)$ for $P^* < P < P_c$.² The transition on crossing P^* can also be seen from $S(T)$; a drop of $S(T)$ at T_c becomes sharper in the pressure range $P^* \leq P < P_c$. T_m from $S(T)$ coincides roughly with that from the $\chi_{ac}(T)$ for $P > P_c$. The transport data in the literature, for example, Refs. 5 and 14, show the $T^{3/2}$ dependence, characteristic of the NFL phase. However, deviation from the $T^{3/2}$ dependence occurs at $T_\rho < T_m$. Therefore, we have relocated the phase boundary of the NFL phase to $T_\rho < T_m$ in Fig. 5

We have made a further analysis of $S(T)$ at ambient pressure and at high pressures. No indication of critical fluctuations has been observed around T_c in the $S(T)$ at ambient pressure. In sharp contrast, under pressure $P > 7$ kbar, the influence of critical fluctuations on $S(T)$ starts at a temperature T_t well above T_c at $P > 9$ kbar. No anomaly of the $S(T)$ is observed at T_0 the on-set temperature for the spin-textured phase detected by neutron inelastic scattering, which indicates that the enhancement of the S is sensitive to the 2D spin fluctuations operative through T_0 . However, a broad maximum in the $S(T)$ under $P > P_c$ occurs at a temperature which is close to T_m found in the ac magnetic susceptibility. In order to further characterize the influence of critical fluctuations on thermoelectric power, we have made a plot of S/T versus $\ln T$ for $S(T)$ under all pressures in Fig. 6. A logarithmic temperature dependence of S/T has been predicted by Paul and Kotliar³² in the vicinity of a QCP. The curve of the paramagnetic phase at ambient pressure pro-

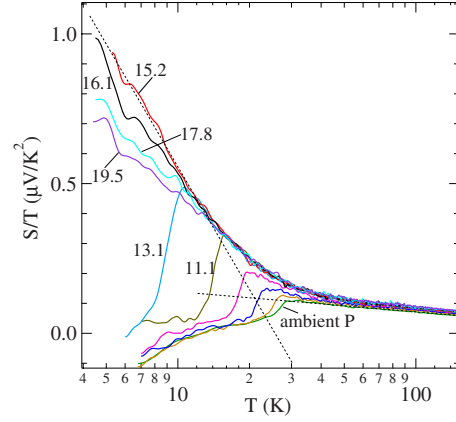


FIG. 6. (Color online) The S/T versus T plot of the $S(T)$ data under different pressures (kbar). Linear fittings have been applied in the paramagnetic phase at $T > T_t$ and at low temperatures where the long-range magnetic order is suppressed.

vides the base line in Fig. 6 without any enhancement. The base line moves up slightly under pressure. Deviation from this line starts at T_t as temperature decreases for pressure $P > 7$ kbar. It is interesting to see from this plot that the enhancement of $S(T)$, as indicated by the absolute value of the slope in S/T versus $\ln T$ at low temperatures, reaches a maximum at a pressure $P \approx P_c$. Although the data are noisy at temperatures near T_m , comparisons between curves under $P > P_c$ indicate that T_m is no longer meaningful in the plot of S/T versus $\ln T$. The low-temperature enhancement of $S(T)$ below T_t can be attributed to quantum critical fluctuations as T_c is reduced and eventually suppressed under pressure. Quantum critical fluctuations are quenched once spins become ordered at T_c in the phase at $P < P_c$. Although the model by Paul and Kotliar is based on two-dimensional antiferromagnetic spin fluctuations, it has been found that the $S/T \propto -\ln T$ relationship works universally in several systems with different magnetic interactions as a QCP is approached by applying a magnetic field in $\text{La}_{1.6-x}\text{Nd}_{0.4}\text{Sr}_x\text{CuO}_4$ ($x = 0.24$) (Ref. 33) where the superconducting phase is suppressed and in $\text{Nb}_{12}\text{O}_{29}$ where the antiferromagnetic order is suppressed,³⁴ or by changing chemical compositions in $\text{Sr}_{1-x}\text{K}_x\text{Fe}_2\text{As}_2$.³⁵ All these systems show an enhanced thermoelectric power due to antiferromagnetic fluctuations near a QCP. It remains to be tested whether the Paul and Kotliar model is applicable in other cases showing ferromagnetic spin fluctuations. In addition, the Kadowaki-Woods ratio of MnSi from this study makes the theoretical treatment for heavy-fermion compounds also applicable to the case of MnSi. A broad spot of the neutron-inelastic scattering intensity along the [110] direction in reciprocal space below T_0 under $P \geq P_c$ indicates not only a spin-ordered structure that is different from the spin-ordered phase below T_c under $P < P^*$, but also the presence of 2D spins fluctuations. A recent muon-spin-relaxation measurement has suggested that the partially ordered spin correlations are dynamic at a time scale between 10^{-11} and 10^{-10} s.³⁶ Although the spin-textured phase has been found at $T < T_0$ and $P < 20$ kbar, the spin-textured phase and 2D spin fluctuations may persist in the phase up to 50 kbar and are responsible for the NFL

phase at low temperatures. Results from this study indicate that the influence of quantum spin fluctuations can be seen at even higher temperatures in the paramagnetic phase over a broad pressure range around P_c .

In conclusion, measurements of transport and magnetic properties under pressure have revealed an abrupt transition from the FL phase to the NFL phase at $P_c \approx 14.6$ kbar. Neutron inelastic scattering studies have further clarified that it is a first-order quantum phase transition from a classic spin-ordered phase to a spin-textured phase with significant 2D quantum spin fluctuations. By measuring the thermoelectric power under high pressure up to 20 kbar, we have shown that quantum spin fluctuations are spread over a broad pressure range around P_c and up to a temperature $T_t > T_m$ where the ac magnetic susceptibility shows a broad maximum. A quantum critical point refers to a second-order magnetic transition that is gradually suppressed to 0 K under high pressure or by applying a high magnetic field. It is normally associated with

physical properties that are strongly influenced by quantum critical fluctuations. The first-order quantum phase transition found at P_c clearly rules out a QCP in MnSi under pressure. However, the high-pressure phase above P_c is not a classic spin-ordered phase. Intrinsic 2D quantum spin fluctuations associated with this spin-textured phase are present at low temperatures in the vicinity of P_c ; they are responsible for a significant enhancement in the thermoelectric power observed in this work. Whether quantum spin fluctuations can also account for the NFL behavior of the transport property deserves reconsideration.

ACKNOWLEDGMENT

This work was supported by NSF (Grant No. DMR 0904282; CBET 1048767) and the Robert A Welch foundation (Grant No. F-1066). J.-S.Z. thanks C. Pfleiderer for insightful discussions.

*jszhou@mail.utexas.edu

- ¹J. D. Thompson, Z. Fisk, and G. G. Lonzarich, *Physica B* **161**, 317 (1989).
- ²C. Pfleiderer, G. J. McMullan, S. R. Julian, and G. G. Lonzarich, *Phys. Rev. B* **55**, 8330 (1997).
- ³C. Pfleiderer, D. Reznik, L. Pintschovius, H. v. Lohneysen, M. Garst, and A. Rosch, *Nature (London)* **427**, 227 (2004).
- ⁴C. Pfleiderer, P. Boni, T. Keller, U. K. RoBler, and A. Rosch, *Science* **316**, 1871 (2007).
- ⁵C. Pfleiderer, S. R. Julian, and G. G. Lonzarich, *Nature (London)* **414**, 427 (2001).
- ⁶C. Pfleiderer, D. Reznik, L. Pintschovius, and J. Haug, *Phys. Rev. Lett.* **99**, 156406 (2007).
- ⁷M. Lee, W. Kang, Y. Onose, Y. Tokura, and N. P. Ong, *Phys. Rev. Lett.* **102**, 186601 (2009).
- ⁸A. E. Petrova, V. Krasnorussky, J. Sarrao, and S. M. Stishov, *Phys. Rev. B* **73**, 052409 (2006).
- ⁹A. E. Petrova, E. D. Bauer, V. Krasnorussky, and S. M. Stishov, *Phys. Rev. B* **74**, 092401 (2006).
- ¹⁰M. Otero-Leal, F. Rivadulla, S. S. Saxena, K. Ahilan, and J. Rivas, *Phys. Rev. B* **79**, 060401(R) (2009).
- ¹¹Y. Ishikawa, K. Tajima, D. Bloch, and M. Roth, *Solid State Commun.* **19**, 525 (1976).
- ¹²P. Bak and M. H. Jensen, *J. Phys. C* **13**, L881 (1980).
- ¹³O. Nakanishi, A. Yanase, A. Hasegawa, and M. Kataoka, *Solid State Commun.* **35**, 995 (1980).
- ¹⁴N. Doiron-Leyraud, I. R. Walker, L. Taillefer, M. J. Steiner, S. R. Julian, and G. G. Lonzarich, *Nature (London)* **425**, 595 (2003).
- ¹⁵C. Pfleiderer (private communication).
- ¹⁶K. Koyama, T. Goto, T. Kanomata, and R. Note, *Phys. Rev. B* **62**, 986 (2000).
- ¹⁷S. M. Stishov, A. E. Petrova, S. Khasanov, G. Kh. Panova, A. A. Shikov, J. C. Lashley, D. Wu, and T. A. Lograsso, *Phys. Rev. B* **76**, 052405 (2007).
- ¹⁸J.-S. Zhou and J. B. Goodenough, *Phys. Rev. B* **54**, 13393 (1996).
- ¹⁹F. P. Mena, D. van der Marel, A. Damascelli, M. Fäth, A. A. Menovsky, and J. A. Mydosh, *Phys. Rev. B* **67**, 241101(R) (2003).
- ²⁰H. Takatsu, H. Yoshizawa, S. Yonezawa, and Y. Maeno, *Phys. Rev. B* **79**, 104424 (2009).
- ²¹S. Junji, *Nippon Butsuri Gakkaishi* **44**, 823 (1989).
- ²²Y. Klein, S. Hebert, A. Maignan, S. Kolesnik, T. Maxwell, and B. Dabrowski, *Phys. Rev. B* **73**, 052412 (2006).
- ²³D. Kim, B. L. Zink, F. Hellman, S. McCall, G. Cao, and J. E. Crow, *Phys. Rev. B* **67**, 100406(R) (2003).
- ²⁴K. Ahn, A. O. Pecharsky, K. A. Gschneidner, and V. K. Pecharsky, *J. Appl. Phys.* **97**, 063901 (2005).
- ²⁵J.-G. Cheng, Y. Sui, J.-S. Zhou, J. B. Goodenough, and W. H. Su, *Phys. Rev. Lett.* **101**, 087205 (2008).
- ²⁶S. M. Stishov, A. E. Petrova, S. Khasanov, G. Kh. Panova, A. A. Shikov, J. C. Lashley, D. Wu, and T. A. Lograsso, *J. Phys.: Condens. Matter* **20**, 235222 (2008).
- ²⁷K. Kadowaki and S. B. Woods, *Solid State Commun.* **58**, 507 (1986).
- ²⁸A. Miyake, A. Villaume, Y. Haga, G. Knebel, B. Salce, G. Lapertot, and J. Flouquet, *J. Phys. Soc. Jpn.* **78**, 044703 (2009).
- ²⁹W. Yu, F. Zamborszky, J. D. Thompson, J. L. Sarrao, M. E. Torelli, Z. Fisk, and S. E. Brown, *Phys. Rev. Lett.* **92**, 086403 (2004).
- ³⁰J.-S. Zhou and J. B. Goodenough, *Phys. Rev. B* **66**, 052401 (2002).
- ³¹C. Pfleiderer, *J. Low Temp. Phys.* **147**, 231 (2007).
- ³²I. Paul and G. Kotliar, *Phys. Rev. B* **64**, 184414 (2001).
- ³³R. Daou, O. Cyr-Choinière, F. Laliberté, D. LeBoeuf, N. Doiron-Leyraud, J.-Q. Yan, J.-S. Zhou, J. B. Goodenough, and L. Taillefer, *Phys. Rev. B* **79**, 180505(R) (2009).
- ³⁴J.-G. Cheng, J.-S. Zhou, J. B. Goodenough, H. D. Zhou, C. R. Wiebe, T. Takami, and T. Fujii, *Phys. Rev. B* **80**, 134428 (2009).
- ³⁵M. Gooch, B. Lv, B. Lorenz, A. M. Guloy, and C. W. Chu, *Phys. Rev. B* **79**, 104504 (2009).
- ³⁶Y. J. Uemura, T. Goko, I. M. Gat-Malueanu *et al.*, *Nat. Phys.* **3**, 29 (2007).